

# Tracking the GMPP of a solar photovoltaic water pumping system with an SMC controller in partial shading conditions

**Sabri Khadija, El Maguiri Ouadia, Farchi Abdelmajid**

Department of Electrical and Mechanical Engineering, Faculty of Science and Technology, University Hassan 1st, Settat, Morocco

---

## Article Info

### Article history:

Received Dec 12, 2022

Revised May 10, 2023

Accepted Jun 5, 2023

---

### Keywords:

Brushless DC motors

Grey wolf optimization

Partial shading condition

Particle swarm optimization

Sliding mode control

---

## ABSTRACT

The focus of this paper will be on the development of a photovoltaic (PV) pumping system that employs a DC-DC boost converter as an intermediate power conditioning unit in a centrifugal water pump powered by a brushless DC (BLDC) motor supplied by a solar photovoltaic panel (SPV). This work describes a particle swarm optimization (PSO) maximum power point tracking (MPPT) method compared with the gray wolf optimizer (GWO) method that are closed-loop with a sliding mode controller (SMC) in order to control the operational point of a solar PV in partial shading conditions (PSC), the DC-DC boost converter provides a low starting current for the BLDC motor, and the voltage source inverter (VSI) is used to perform electronic commutation of the BLDC motor. Furthermore, the BLDC motor's speed is regulated by the changeable DC link voltage. The system under consideration, as well as the control approaches employed, were created in the MATLAB/Simulink environment.

*This is an open access article under the [CC BY-SA](#) license.*



---

## Corresponding Author:

Sabri Khadija

Department of Electrical and Mechanical Engineering, Faculty of Science and Technology

University Hassan 1st

Settat, Morocco

Email: k.sabri@uhp.ac.ma

---

## 1. INTRODUCTION

Rural and remote areas where there is no access to electricity networks, suffer from an increased lack of water. This shortage has led to a growing interest in the use of photovoltaic (PV) generators as an energy source. Indeed, the practical and cost-effective solution to the problem of water scarcity is to implement a stand-alone PV pumping system. Motors absorb more than 40% of the energy consumed in driving systems. As a result, motors are critical in applications requiring electric drives, such as pumping water in a solar system [1]. Induction motors AC first drew a lot of attention for water pumping systems [2], [3] due to its simplicity, low construction cost, and low maintenance. However, as speed increases, brush friction necessitates more precise control, reducing useful torque [4]. The hunt for a superior substitute for induction motors led to the creation of brushless DC (BLDC) motors. In this regard BLDC motors have become popular in the automotive, robotics, and medical industries in this respect. These motors have several advantages over other types of motors, including silent operation, extended life, excellent efficiency owing to smooth speed control, enhanced power density, and reduced electromagnetic interference [1], [5].

The power efficiency of the gross premium valuation (GPV) has a major influence on the performance of a PV pumping system. Because PV systems are non-linear, the use of an maximum power point tracking (MPPT) control rule is required to assure maximum power transfer to the load [4]. Several MPPT approaches are available in the literature to reach this maximum power point (MPP) [6]–[8]. Among the most commonly used traditional approaches are the perturb and observe (P&O) method, the incremental conductance (INC)

method, the fractional short circuit, and the fractional open voltage circuit [7], [8]. However, because the MPP varies with sunshine and season, it is difficult to keep this sort of MPP tracker running. There was a considerable loss of electricity. Due to the difficulty in detecting the precise MPP when the P-V characteristics include several peaks [9], [10], the system has become less efficient under changing irradiation conditions [11]. To solve this problem, many improved MPPT algorithms, fuzzy logic, and artificial intelligence-based systems have been created, in order to assess the system's dynamic reactivity, and provide better MPP monitoring. This work describes a particle swarm optimization (PSO) method compared with the gray wolf optimizer (GWO) method that have closed-loop with a sliding mode control (SMC) for a weather-aware PV water pumping system. SMC is recommended as a particularly suitable approach to cope with variations in solar radiation for PV system operation [11], [12]. In general, the selection of DC-DC converters is critical in defining the best performance of BLDC drives, and as a result, enhancing the output of the renewable energy system [3]. In the PV system, various types of DC-DC converters, such as buck, boost, buck boost, cuk, and single ended primary inductor converter (SEPIC) [3], [8], [9], [13], [14], are implemented with the following considerations in mind: high output voltage gain, low input current, low current ripples, higher efficiency, minimal cost, higher efficiency, high maximum power flow, and easy system drive [15]. Figure 1 shows a schematic design of the investigated water pumping system. This system is made up of PV solar panels, a boost DC-DC converter, a three-phase inverter voltage source inverter (VSI) operated BLDC motor and a centrifugal pump.

The following is an excerpt from this article: in section 1, there is an introduction. Section 2 presents the studied system's configuration (solar photovoltaic panel (SPV) network, DC-DC boost converter, BLDC motor, and centrifugal pump). Section 3 presents the studied system's control (PSO and GWO algorithms and SMC). Section 4 presents the results and analysis using the MATLAB/Simulink environment and conclusion in section 5.

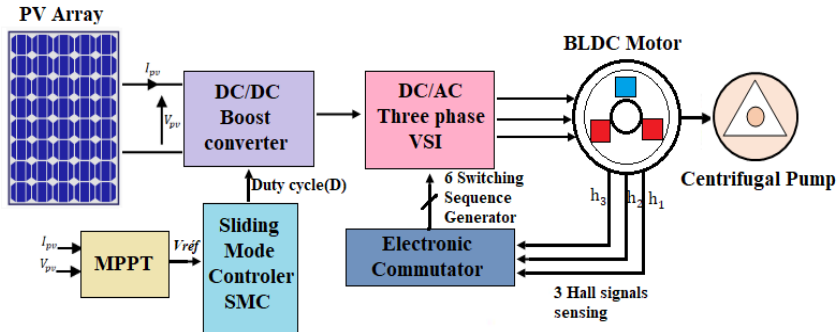


Figure 1. Solar pumping system design

## 2. SYSTEM DISCRIPTION

### 2.1. Photovoltaic panel

PV module efficiency varies with the quantity of light received. Figure 2 depicts the corresponding circuit model of a solar cell [9] and is characterised by (1)-(4):

$$I_{pv} = I_{ph} - I_s \left[ e^{\left( \frac{q(V_{pv} + I_{pv}R_s)}{AN_s K T} \right)} - 1 \right] - \frac{V_{pv} + I_{pv}R_s}{R_{sh}} \quad (1)$$

$$I_{ph} = [I_{ph0} + J_i(T - T_{sc})] \frac{E}{E_{sc}} \quad (2)$$

$$I_s = I_{so} \left( \frac{T}{T_{sc}} \right)^3 e^{\frac{qE_{gap}}{A \cdot K} \left( \frac{1}{T_{sc}} - \frac{1}{T} \right)} \quad (3)$$

$$I_{so} = \frac{I_{ph0}}{e^{\frac{qV_{oc}}{A \cdot K \cdot N_s \cdot T_{sc}}} - 1} \quad (4)$$

With  $I_{pv}$  and  $V_{pv}$  are respectively the PV panel current and voltage,  $N_s$  is the number of PV module cells,  $K$  is the Boltzmann constant ( $1.3806503e-23$  J/K),  $T$  is the cell temperature in Kelvin,  $q$  is the electron charge ( $1.60217646e-19$  C),  $I_{so}$  is the saturation current at  $T_{sc}$ ,  $I_{ph0}$  is the photo-current measured under the standard conditions  $E_{sc}$ ,  $T_{sc}$  ( $E_{sc} = 1,000$  W/m<sup>2</sup> and  $T_{sc} = 25$  °C), and  $J_i$  is the temperature coefficient of the short circuit-

current. The key parameters for utilizing this model in simulation are shown in Table 1. To illustrate the behavior of the PV model, the current-voltage and power-voltage curves of the model for different irradiation values at constant temperature ( $25^\circ$ ) are shown in Figure 3.

PV module efficiency varies with the quantity of light received as presented in Figure 4(a). As a result, it is critical to investigate the qualities of a PV module under various irradiation scenarios, such as uniform irradiation and partial shading conditions (PSC), where multiple local and global MPPs may be seen on the P-V characteristics curve [6], [10] as seen in Figure 4(b). The use of bypass diodes linked in parallel to each PV module during PSCs reduces the possibility of a hot spot, in which the shaded module works as a load rather than generating power [16]. The top peak in Figure 4(b) for the PV array is the global peak, which is successively equivalent to 188.53 W for profile 1 and 131.89 W, while the others are local peaks.

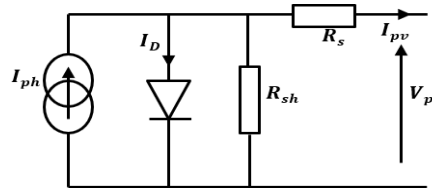


Figure 2. Single diode circuit of a PV module

Table 1. Parameters of the PV array

Parameters	Nomenclature	Values
Voltage at open cct	$V_{oc}$	21.7 V
Short cct-current	$I_{sc}$	7.3 A
Max power voltage	$V_{mpp}$	32.82 V
Max power current	$I_{mpp}$	8.07 A
Photo-current	$I_{ph}$	8,6307 A
Saturation current	$I_s$	$1.4176e^{-10}$ A
Diode ideality	$A$	0.99132
Series resistance	$R_s$	0.098625 $\Omega$
Shunt resistance	$R_{sh}$	82.1161 $\Omega$
Bandgap's energy	$E_{gap}$	1.12 eV

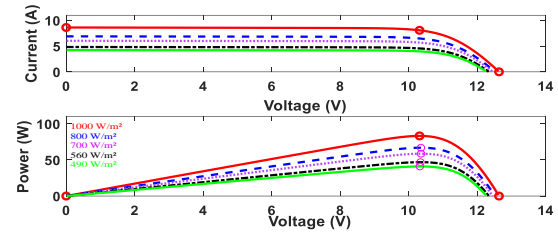
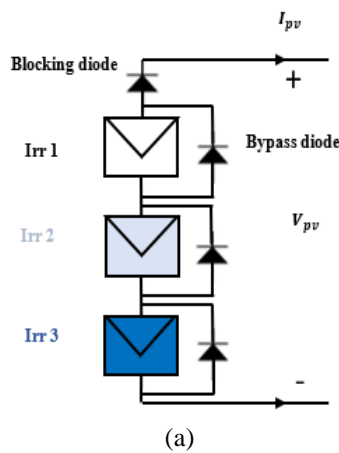
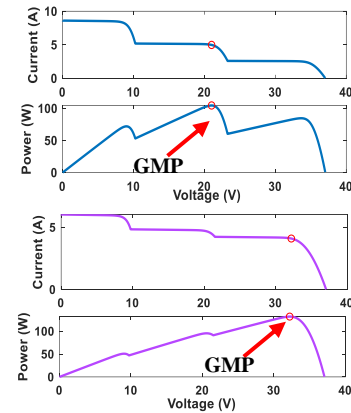


Figure 3. The current-voltage and power-voltage curves of the model



(a)



(b)

Figure 4. Under PSC: (a) structure of the PV panel and (b) the I-V and P-V characteristics of the PV panel

## 2.2. DC-DC boost converter design

Choosing DC-DC converters in general is the best approach for determining the optimal performance of BLDC motors and therefore optimizing solar system production. Indeed, the SMC is designed to follow the voltage reference  $V_{ref}$  by adjusting the duty cycle of this DC-DC boost converter. Figure 5 is an example of a boost converter, and its average model is given by (5):

$$\begin{cases} \frac{dV_{pv}}{dt} = \frac{1}{C_1} (I_{pv} - I_L) \\ \frac{dI_L}{dt} = \frac{1}{L} (V_{pv} - (1 - V_{ref})V_s) \\ \frac{dV_s}{dt} = \frac{1}{C_2} (I_L(1 - V_{ref}) - I_s) \end{cases} \quad (5)$$

The relation between the input and output voltages is shown in (6):

$$\frac{V_s}{V_{pv}} = \frac{1}{1 - V_{ref}} \quad (6)$$

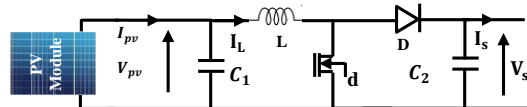


Figure 5. The boost converter circuit

### 2.3. Modeling of brushless DC motors, commutation, and voltage source inverter switching

BLDC motor is also called electronically commutated motor [7], [8], [13]. This electric actuator is said to be the best for solar pumping in Figure 6. The main purpose of electronic commutation is to operate a VSI in such a way that the DC current drawn from the DC link capacitor is symmetrically placed over  $120^\circ$  in the center of each phase. To achieve this, the rotor position must be monitored at each switching time, i.e., every 60 electrical degrees or six times in an electrical cycle. To do this, the position information is taken by a position sensor, often a hall sensor [17]. When the magnetic poles of the rotor approach the hall sensors, they create a separate set of three hall signals ( $h_1$ ,  $h_2$ , and  $h_3$ ). These signals are digital in nature and are logically transformed into six switching pulses ( $s_1$ ,  $s_2$ ,  $s_3$ ,  $s_4$ ,  $s_5$ , and  $s_6$ ) that are used to control the VSI switches [14], [18].

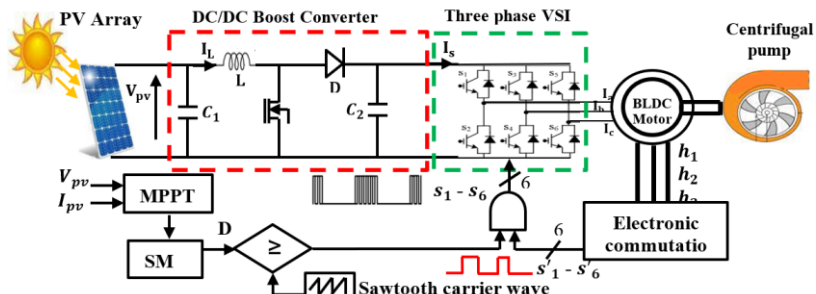


Figure 6. Configuration of the proposed SPV array and boost converter powered by a BLDC motor for a water pumping system

The comparison of the duty cycle generated by the MPPT/SMC assembly with a high frequency sawtooth carrier wave (to keep the symmetry) gives us a high frequency pulse width modulation (PWM) pulse. A logic AND gate is used for fundamental frequency modulation [8], [14]. As an example, the conduction states of two switches ( $s_1$  and  $s_4$ ) of a VSI supplying a BLDC motor are shown in Figure 7.

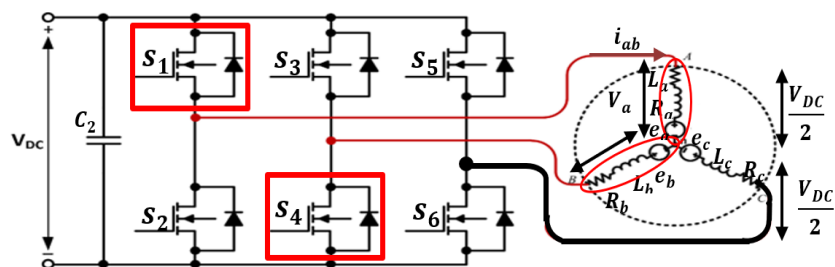


Figure 7. A BLDC motor powered by a VSI during the conduction states of ( $s_1$  and  $s_4$ )

The MPPT algorithm generates a duty cycle for the VSI, which controls the link voltage  $V_{DC}$ . Then, as the atmospheric conditions change, so does the power supply by the PV and the speed of the BLDC motor [13], [18]. The role of power conditioning is to maximize the energy transfer between the PV array and the pumping unit. The power conditioning is provided by a DC/AC inverter. The three-phase inverter voltages ( $V_a$ ,  $V_b$ , and  $V_c$ ) are represented by (7)-(9) [15]. It should be noted that the BLDC motor stator phase currents ( $i_a$ ,  $i_b$ , and  $i_c$ ), flux links ( $\lambda_a$ ,  $\lambda_b$ , and  $\lambda_c$ ), and back emfs ( $e_a$ ,  $e_b$ , and  $e_c$ ) have trapezoidal waveforms [13], [19].

$$\begin{aligned} V_a &= R_a i_a + \lambda_a + e_a \quad \text{with} \quad \lambda_a = (L_a - L_m) \frac{di_a}{dt} \\ V_b &= R_b i_b + \lambda_b + e_b \quad \text{with} \quad \lambda_b = (L_b - L_m) \frac{di_b}{dt} \\ V_c &= R_c i_c + \lambda_c + e_c \quad \text{with} \quad \lambda_c = (L_c - L_m) \frac{di_c}{dt} \end{aligned} \quad (7)$$

Where  $R_{a,b,c}$  are winding resistance of stator winding,  $L_{a,b,c}$  are self-inductance of each phase of the stator winding, and  $L_m$  is mutual inductance in any two phases. The back electromotive force is represented in (8), as a function of the rotor position  $\theta$  at flux  $\lambda$ , and speed  $\omega_r$ . It is worth noting that  $f(\theta)$  has the same trapezoidal shape as the counter-electromotive force per phase [20], where x represents the three phases (a, b, or c).

$$e_x = f(\theta) \lambda_x \omega_r \quad (8)$$

The BLDC motor's output electromagnetic torque  $T_{emc}$  is determined from the output power  $P_s$  and the mechanical rotor speed is  $\omega_r$  [13], provided in (9):

$$T_{emc} = \frac{P_s}{\omega_r} = \frac{\sum e_x i_x}{\omega_r} \quad (9)$$

The BLDC motor in our proposed system is connected to a centrifugal pump via its shaft [18]; the choice of this type of pump is related to its ability to operate at its rated speed and power for long periods of time even in the presence of partial shading, and thus its ability to pump a large volume of water while delivering a relatively high overall system efficiency. Water pumping necessitates a torque  $T_p$  proportional to the square of the motor speed  $\omega_r$ . The characteristic torque looks (10) [19], [21]:

$$T_p = K_p \omega_r^2 \quad (10)$$

### 3. MAXIMUM POWER POINT TRACKING CONTROL TECHNIQUES

#### 3.1. Particle swarm optimization

In the search space of a PSO system, flies a swarm of individuals (particles) that represent a candidate solution to the optimization problem [22]. Each particle is fully characterized in terms of position  $z_i$  and velocity  $\phi_i$  as shown in (11) and (12). Initially, the particles are randomly initialized in the search space of the problem. Then, at each iteration, each particle moves and uses two final values to update their positions and velocities [23], [24]. The flowchart of the MPPT-based PSO is given in Figure 8(a).

$$z_i^{k+1} = z_i^k + \phi_i^{k+1} \quad (11)$$

$$\phi_i^{k+1} = w \phi_i^k + m_1 r_1 (P_{best} - z_i^k) + m_2 r_2 (G_{best} - z_i^k) \quad (12)$$

Where,  $w$  is called the inertia weight,  $m_1$  and  $m_2$  considered as acceleration coefficients,  $r_1$  and  $r_2$  as random variables uniformly distributed within  $[0, 1]$ ,  $k$  is the iteration number,  $P_{best}$  is as the personal best position of particle, and  $G_{best}$  is called the best position of the particles for entire swarm population [23].

The reference voltage and output power of the PV system are determined sequentially by the position and velocity of the particle swarm when using the PSO approach in the MPPT domain [22]. As a result, (11) may be changed as (13):

$$V_{ref,i}^{k+1} = V_{ref,i}^k + P_{s,i}^{k+1} \quad (13)$$

Indeed, after each cycle, the particle with the greater power remains fixed in its position, while the other particles move in accordance with the position  $x_i$ . Finally, after the required global maximum has been obtained, the ideal voltage is saved and returned as the output signal to be tracked PWM. The PSO optimizer runs as long as the

load requires power [25]–[27]. Clearly, changes in air conditions have an impact on power production and voltage. As a result, as (14) and (15) is used to validate the detection of fluctuations in power and voltage [27]:

$$\left| \frac{P_{s,i} - P_{s,(i-1)}}{P_{s,i}} \right| \geq \Delta P_{set} \quad (14)$$

$$|V_{réf,i} - V_{réf,(i-1)}| \leq \Delta V_{set} \quad (15)$$

Where  $\Delta P_{set}$  and  $\Delta V_{set}$  are the power and voltage thresholds, respectively. These ones are predetermined by the user (i), (i-1): the current and the previously measured values, respectively. The parameters of the PSO algorithm employed in our study are  $w=0.1$ ,  $m_1=m_2=1.2$ ,  $ra_1=ra_2=0.5$ , size of population is 5, and dimension number is 1.

### 3.2. Grey wolf optimization

GWO is a novel meta-heuristic algorithm inspired by grey wolves. The wolves in the pack are classified into four types based on their physical shape and strength: alpha ( $\alpha$ ), beta ( $\beta$ ), delta ( $\delta$ ), and omega ( $\omega$ ) [5], [28]. The GWO utilized (16)–(19) [29] and the flowchart of the proposed GWO-based MPPT algorithm is shown in Figure 8(b).

$$D = |C \cdot X_p(j) - X_p(j)| \quad (16)$$

$$X(j+1) = X_p(j) - A \cdot D \quad (17)$$

$$A = 2ab_1 - a \quad (18)$$

$$C = 2 \cdot b_2 \quad (19)$$

Where  $j$  is the current iteration;  $D$ ,  $A$ , and  $C$  are the coefficient vectors;  $X_p$  is the position of the prey;  $X$  is the position of grey wolf;  $a$  is a variable which linearly decreased from 2 to 0 over course of iterations that resembles approaching the prey, and  $b_1$ ,  $b_2$  are a random variable whose value is [0-1].

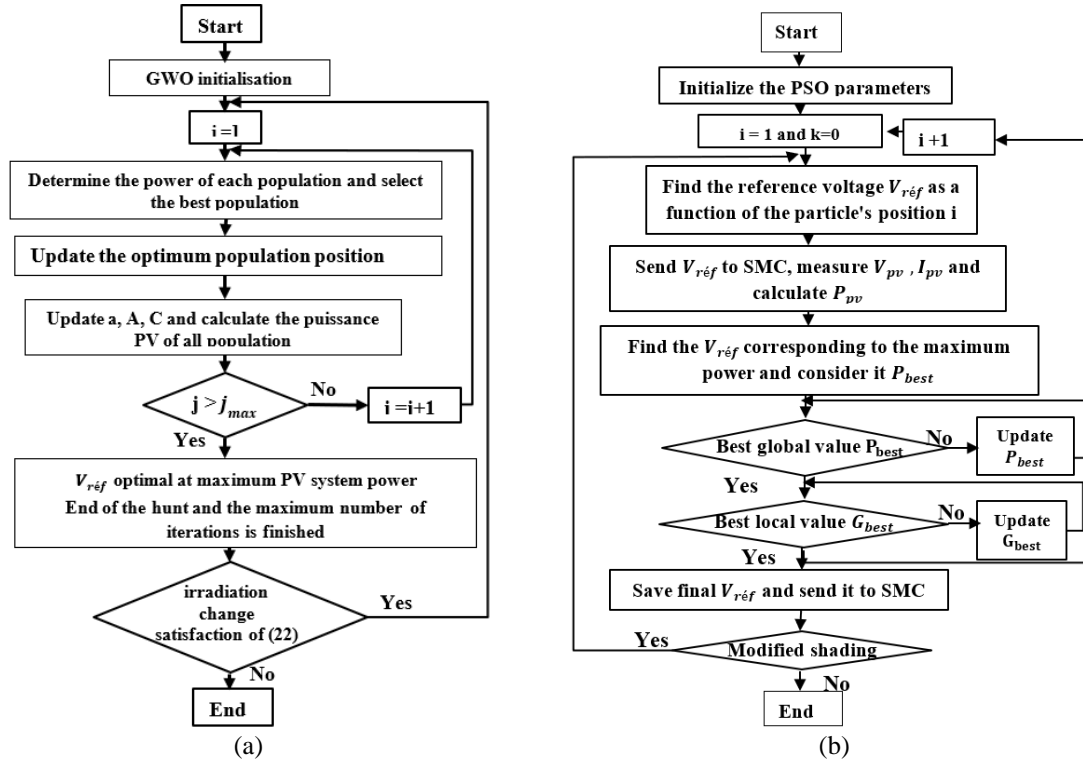


Figure 8. Flowchart for (a) PSO MPPT algorithm and (b) GWO MPPT algorithm

When using the GWO approach to track maximum power, the reference voltage  $V_{réf}$  is specified as a gray wolf in this paper as shown in (20). Firstly, it is necessary to initialize the population (number of wolves) in our case it is considered three (the number of PV module) by setting minimum and maximum limits, then we calculate the PV power that determines the fitness value of the wolves, by determining two values as first and second maximum power. The search ends when the maximum PV power is obtained (the prey stops moving) after updating the positions. Each change of irradiation allows to reinitialize the search by validating as (21) [28], [30].

$$V_{réf}(j+1) = V_{réf}(j) - A \cdot D \quad (20)$$

$$\left| \frac{P_{pv} - P_m}{P_m} \right| \geq \Delta P \quad (21)$$

Where  $P_m$  is the current global MPP of the panel. In the case of PSC,  $P_{pv}$  will be much lower than  $P_m$  and  $\Delta P$  is set at 0.05 to have better performance.

### 3.3. Sliding mode controller design

The SMC is a type of controller applied to non-linear systems, known for its robustness and ease of implementation compared to other non-linear control techniques [31]. A typical SMC includes two operating modes (bisectional). First, the sliding surface must be chosen in such a way that the system dynamics are stable, and then a control must be designed to make the switching surface appealing to the system state [27], [32], [33] as (22):

$$\begin{cases} y = V_{pv} \\ y_{réf} = V_{réf} \end{cases} \quad (22)$$

The tracking error  $\mathcal{E}$  is (23):

$$\mathcal{E} = y - y_{réf} \quad (23)$$

First, the sliding surface defined as (24):

$$S = \left( \Psi + \frac{d}{dt} \right) \mathcal{E}^{r-1} \quad (24)$$

With  $\Psi$  is the positive constant, and  $r$  is the relative degree E. The derivative of output  $y$  is (25):

$$\dot{y} = \dot{V}_{pv} = \frac{1}{C_1} I_{pv} - \frac{1}{C_1} I_L \quad (25)$$

Using (3) and (6), the second derivative of  $y$  can be represented as (26):

$$\ddot{y} = \ddot{V}_{pv} = \frac{1}{C_1} \dot{I}_{pv} - \frac{1}{LC_1} (V_{pv} - (1-d)V_s) \quad (26)$$

As can be seen, the second derivation of  $y$  results in the appearance of the law control, which is the duty cycle  $d$  of the DC/DC boost converter. As a result, the relative degree  $r$  would be 2. Therefore, the sliding surface displayed in (24) will be (27):

$$S = \left( \Psi + \frac{d}{dt} \right) \mathcal{E} \quad (27)$$

Its time derivative is expressed as (28):

$$\dot{S} = \Psi \dot{\mathcal{E}} + \ddot{\mathcal{E}} \quad (28)$$

Where the second time derivative is expressed as (29):

$$\ddot{\mathcal{E}} = \ddot{y} - \ddot{y}_{réf} = \ddot{V}_{pv} - \ddot{V}_{réf} \quad (29)$$

By substituting (5) for (29):

$$\ddot{\mathcal{E}} = \frac{1}{C_1} \dot{I}_{pv} - \frac{1}{LC_1} (V_{pv} - (1-d)V_s) - \ddot{V}_{réf} \quad (30)$$

Assuming  $\dot{V}_{ref}$  and  $\ddot{V}_{ref}$  set to zero, the time derivative of the sliding mode surface is (31):

$$\dot{S} = \lambda \dot{V}_{pv} + \frac{1}{C_1} \dot{I}_{pv} - \frac{1}{LC_1} (V_{pv} - (1-d)V_s) \quad (31)$$

The stability of the system can be obtained via the analysis of the Lyapunov theory defined positively as (32):

$$V = \frac{1}{2} S^2 \quad (32)$$

It is only necessary that the derivative with respect to time of the Lyapunov function is negative while the coefficient  $k$  must be positive (33):

$$\dot{V} = S \dot{S} = -k \text{sign}(S) \quad (33)$$

The convergence to zero in finite time of the sliding surface assures that the system will be asymptotically stable, the first-time derivative of  $S$  should be (34):

$$\dot{S} = -k \text{sign}(S) = \lambda \dot{V}_{pv} + \frac{1}{C_1} \dot{I}_{pv} - \frac{1}{LC_1} (V_{pv} - (1-d)V_s) \quad (34)$$

The duty cycle control  $d$  can be found as (35):

$$d = \frac{LC_1}{V_s} \left[ k \text{sign}(S) + \dot{V}_{pv} + \frac{1}{C_1} \dot{I}_{pv} \right] - \frac{V_{pv}}{V_s} + 1 \quad (35)$$

#### 4. SIMULATION RESULTS AND DISCUSSION

The setup under consideration in this study consists of three PV modules linked in series, each with 20 cells as shown in Figure 9, the selected module is AMETEK. MATLAB/Simulink was used to analyze the performance of the proposed system discussed in section 2. Table 1 shows the SPV specification and Table 2 shows the boost converter parameter that was utilized to power the BLDC motor-water pump (TETRA 142TR12 series) are defined in Table 3. Two irradiation profiles have been considered in this study: profile 1 is the three PV modules receive initially between [0,1 s] an irradiation of 800 W/m<sup>2</sup>, 700 W/m<sup>2</sup>, and 1,000 W/m<sup>2</sup> at 25 °C and profile 2 is between [1 s, 2 s] they receive 560 W/m<sup>2</sup>, 490 W/m<sup>2</sup>, and 700 W/m<sup>2</sup> at 25 °C. It should be noted that these shifts are sudden, which is not realistic in practice.

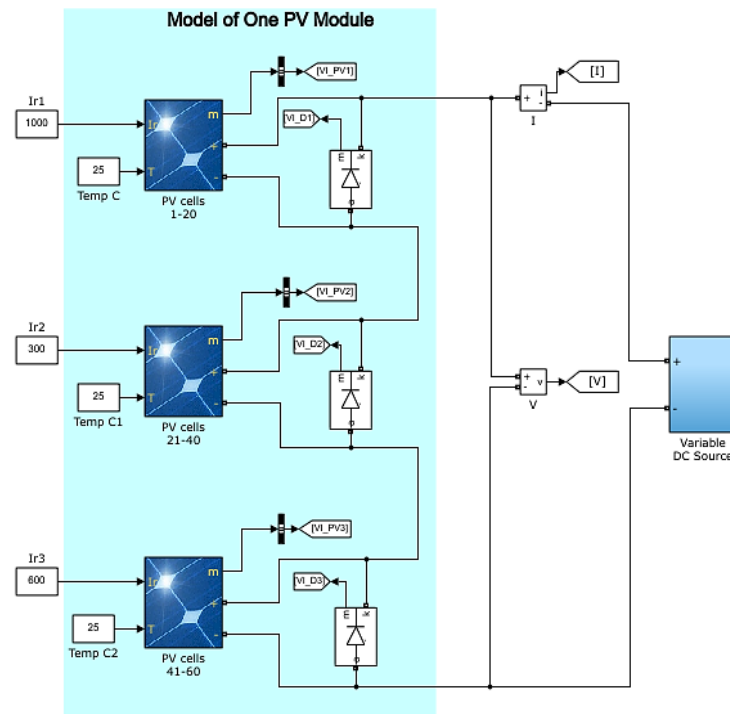


Figure 9. Model of partially shaded PV panels

Table 2. The three-phase inverter's switched states

Intervals	Hall signals			Electronic commutation					
	$h_1$	$h_2$	$h_3$	$s_1$	$s_2$	$s_3$	$s_4$	$s_5$	$s_6$
NA	0	0	0	0	0	0	0	0	0
0-60	0	1	1	0	0	0	1	1	0
60-120	1	1	0	0	1	1	0	0	0
120-180	1	0	1	0	1	0	0	1	0
180-240	1	0	1	1	0	0	0	0	1
240-300	1	1	0	1	0	0	1	0	0
300-360	0	1	1	0	0	1	0	0	1

Table 3 .Parameters of BLDC motor

Parameters	Values
Stator phase resistance	2.3 $\Omega$
Stator phase inductance	0.05e-3 H
Rated power	200 W
Rated speed	600 rpm
Voltage constant	11 V/krpm
Flux linkage	0.052521 V/s
Inertia	0.0008 kg.m <sup>2</sup>
Viscose dumping	0.001 N.m.s
Pole pairs	1
Torque constant	0.10504 N.m/A

#### 4.1. Performance of solar PV array

The two irradiance profiles considered in this paper are shown in Figure 10(a). A strong ripple in MPP voltage and power can be observed when PSO and GWO MPPT techniques are implemented, as shown in Figures 10(b) and (c), respectively. The PSO MPPT technique expects a voltage of 32.95 V, while that achieved by GWO is 32.66 V. The maximum power seen in the two MPPT methods proposed in this work is 186.3 W (PSO and GWO). Because the system under consideration begins with a radiation of 700 W/m<sup>2</sup>, there are high transients induced by the GWO method at all levels of irradiation in the profile 1, resulting in a significant loss of power. When the shade pattern changes in profile 2, a new P-V curve is depicted in Figure 10(b), and both algorithms search the P-V curve for a new MPP. The combined maximum power of the two systems shown is 104 W. The PSO method allows for a 0.3 s stabilization time to attain the MPP in the transient state during [0-1 s]. The graphs of voltage and PV power are zoomed in on the 0.2-1 s intervals to highlight the transient and steady state ripples, respectively. During the interval [1,2], both methods exhibit the same performance and voltage and maximum power levels. As the irradiance changes, the SPV array's power tracking improves dramatically. Under shifting climatic circumstances, the MPPT approaches clearly optimize the SPV array power.

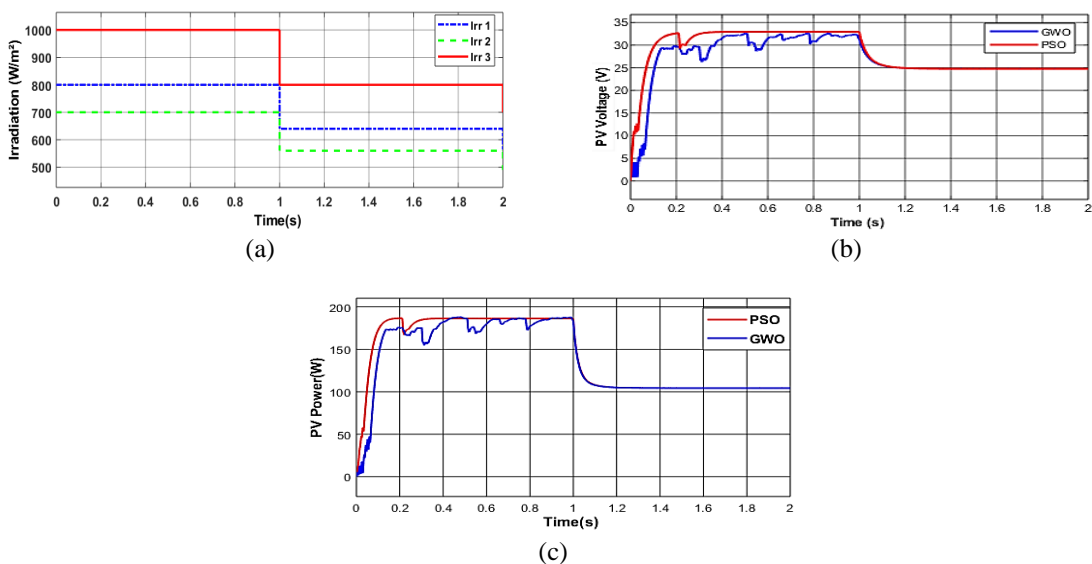


Figure 10. Performance of SPV array under PSC: (a) irradiance profile, (b) PV generator voltage, and (c) PV generator power

#### 4.2. Performance of DC-DC boost converter

The performance of the boost converter is shown in Figures 11(a) and (b). They are associated with the duty cycle in Figures 11(c) and (d). The continuous conduction mode of operation is maintained even when the irradiance varies. Boost's conductance current  $I_L$  is 5.8 A when PSO MPPT is used, and it increases from 4.72 A to 5.76 A when GWO is used for [0-1 s]. The  $I_L$  conductance current is 4.22 A for the second profile between [1-2 s], according to both MPPT algorithms investigated. The DC link voltage is represented by the boost output voltage  $V_s$ , varies from a low of 23 V during [1-2 s] to a high of 32 V during profile 1 [0-1 s]. When compared to the GWO approach, the PSO algorithm greatly reduces the ripple content of the inductor current and link voltage.

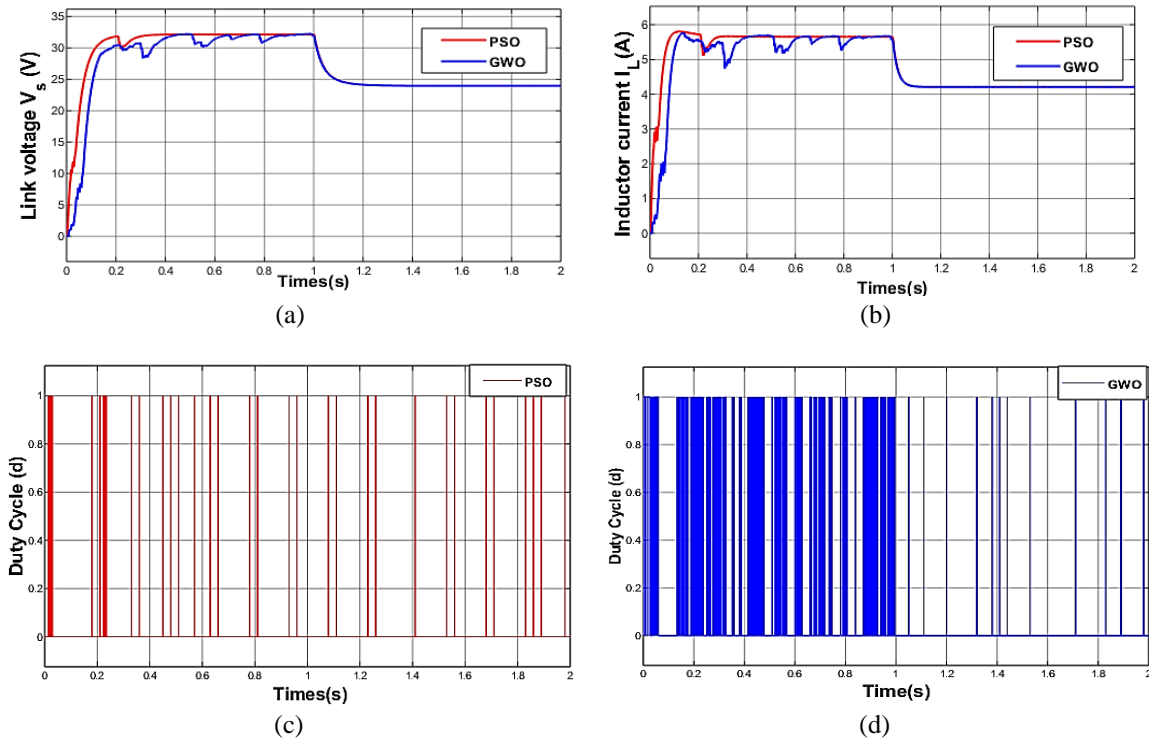


Figure 11. Boost performance when implementing the PSO and GWO MPPT techniques: (a) link voltage  $V_s$  (s), (b) inductor current  $I_L$ , (c) duty cycle for PSO MPPT, and (d) duty cycle for GWO MPPT

#### 4.3. Performance of BLDC motor-pump

Figures 12(a)-(d) (in Appendix) for GWO MPPT and Figures 13(a)-(d) (in Appendix) for PSO MPPT show the BLDC motor parameters. In the first profile, the BLDC motor reaches its maximum speed of 522 rpm in 0.4 s using PSO MPPT, while the GWO algorithm require 0.5 s. Due to electronic commutation, the BLDC motor creates electromagnetic torque with pulsations. The PSO MPPT method generates the least torque ripple. The soft-switching technique regulates the motor stator current via the DC-DC boost, and it achieves the rated intermediate circuit current of 5.78 A in 0.08 s.

The PSC slows down the pace in the second profile. The waveform in Figures 11(c) and 13(c) shows that the BLDC motor achieves 399 rpm using both approaches given. The motor may also run at 50% of the irradiance, or 500 W/m<sup>2</sup>. As illustrated in Figures 12(d) and 13, the speed and electromagnetic torque may smoothly follow irradiance fluctuations. Due to the electrical switching of the VSI, pulses can be seen in the electromagnetic torque of the BLDC motor Figure 12(d).

## 5. CONCLUSION

This study describes how to use SMC theory on a DC-DC boost converter to power a water pump with a BLDC motor under various climatic circumstances. The flexible control provided by PSO and GWO MPPT has enabled the intelligent and efficient operation of the solar water pumping system via the boost to satisfy the initial objectives of MPPT extraction, smooth speed variation, and soft starting of a BLDC motor. The designed controller was able to predict the duty cycle for the boost converter to extract the maximum available PV power and ensure the soft start of the BLDC motor. The transient and steady state performance

of the PSO MPPT method compared with GWO reveals that the power tracking efficiency of the PSO MPPT algorithm is the highest.

## APPENDIX

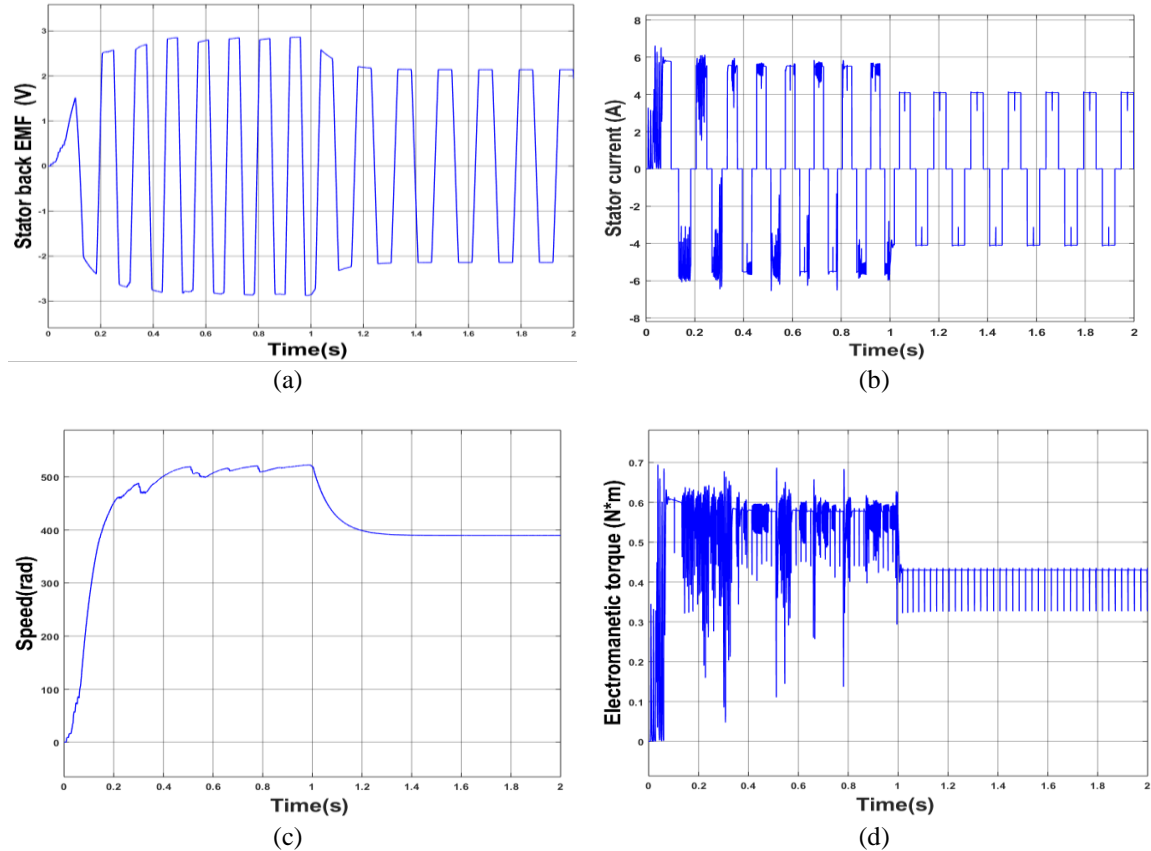


Figure 12. Performance of BLDC motor-pump under variable solar irradiation with GWO algorithm:  
(a) back emf  $e_a$ , (b) stator current  $I_a$ , (c) stator speed  $\omega_r$ , and (d) electromagnetic torque  $T_e$

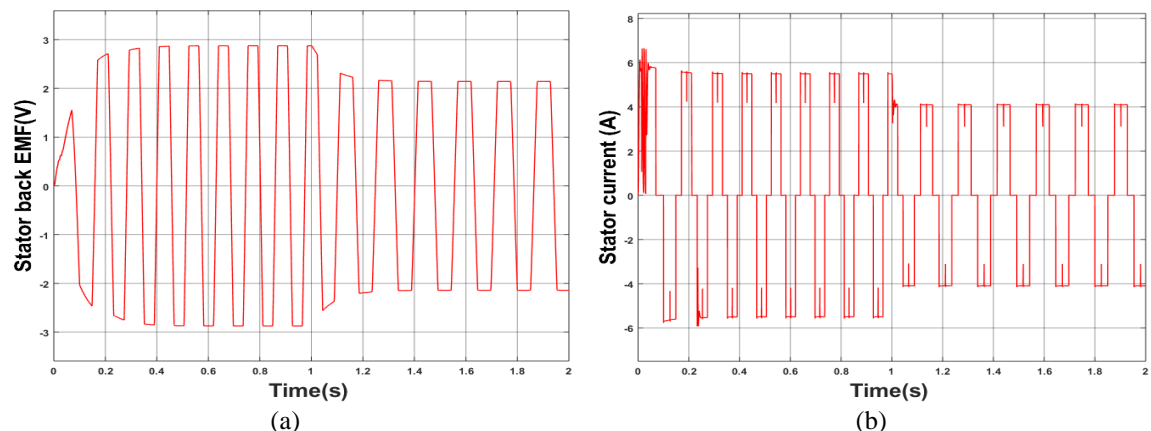


Figure 13. Performance of BLDC motor-pump under variable solar irradiation with PSO algorithm:  
(a) back emf  $e_a$ , (b) stator current  $I_a$

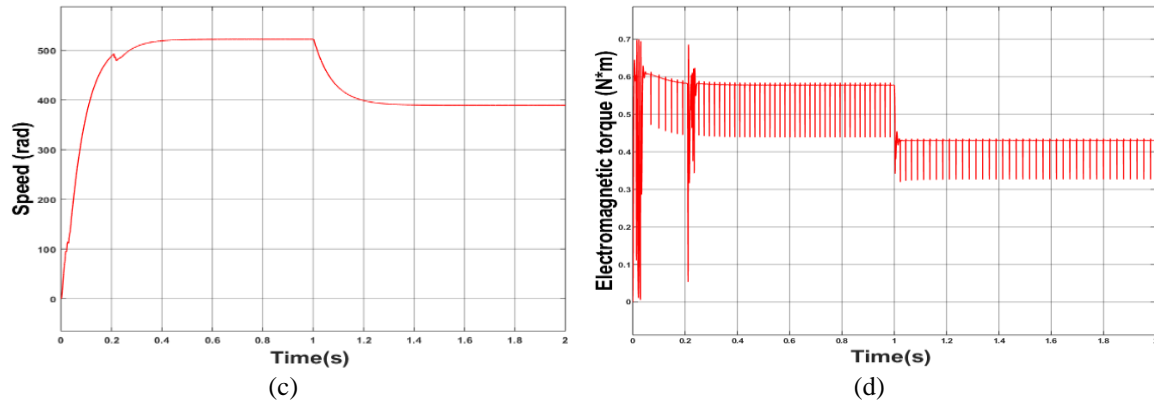


Figure 13. Performance of BLDC motor-pump under variable solar irradiation with PSO algorithm:  
(c) stator speed  $\omega_r$  and (d) electromagnetic torque  $T_e$  (continue)

## REFERENCES

- [1] R. Nisha and K. G. Sheela, "Review of PV fed water pumping systems using BLDC Motor," *Mater. Today Proc.*, vol. 24, pp. 1874–1881, 2019, doi: 10.1016/j.mtpr.2020.03.612.
- [2] M. Errouha and A. Derouich, "Study and comparison results of the field oriented control for photovoltaic water pumping system applied on two cities in Morocco," *Bull. Electr. Eng. Informatics*, vol. 8, no. 4, pp. 1206–1212, 2019, doi: 10.11591/eei.v8i4.1301.
- [3] H. R. Khoei and M. Zolfaghari, "New Model Reference Adaptive System Speed Observer for Field-Oriented Control Induction Motor Drives Using Neural Networks," *Bull. Electr. Eng. Informatics*, vol. 5, no. 1, pp. 25–36, 2016, doi: 10.11591/eei.v5i1.520.
- [4] M. Benzaouia, L. Bouselham, B. Hajji, A. M. Dubois, A. Benslimane, and M. El Ouariachi, "Design and Performance Analysis of a Photovoltaic Water Pumping System based on DC-DC Boost Converter and BLDC Motor," *Proc. 2019 7th Int. Renew. Sustain. Energy Conf. IRSEC 2019*, pp. 5–10, 2019, doi: 10.1109/IRSEC48032.2019.9078267.
- [5] A. D. G. Jegha, M. S. P. Subathra, N. M. Kumar, U. Subramaniam, and S. Padmanaban, "A high gain DC-DC converter with grey wolf optimizer based MPPT algorithm for PV fed BLDC motor drive," *Appl. Sci.*, vol. 10, no. 8, pp. 1-2020, doi: 10.3390/APP10082797.
- [6] K. Sabri, O. E. Maguiri, and A. Farchi, "Comparative Study of Different MPPT Algorithms for Photovoltaic Systems under Partial Shading Conditions," *2021 9th International Renewable and Sustainable Energy Conference (IRSEC)*, 2021, pp. 1-7, doi: 10.1109/IRSEC53969.2021.9741164.
- [7] N. Priyadarshi, S. Padmanaban, L. Mihet-Popa, F. Blaabjerg, and F. Azam, "Maximum power point tracking for brushless DC motor-driven photovoltaic pumping systems using a hybrid ANFIS-FLOWER pollination optimization algorithm," *Energies*, vol. 11, no. 5, pp. 1-16, 2018, doi: 10.3390/en11051067.
- [8] R. Kumar and B. Singh, "Single Stage Solar PV Fed Brushless DC Motor Driven Water Pump," *IEEE J. Emerg. Sel. Top. Power Electron.*, vol. 5, no. 3, pp. 1377–1385, 2017, doi: 10.1109/JESTPE.2017.2699918.
- [9] A. A. Alzubaidi, L. A. Khaliq, H. S. Hamad, W. K. Al-Azzawi, M. S. Jabbar, and T. A. Shihab, "MPPT implementation and simulation using developed P&O algorithm for photovoltaic system concerning efficiency," *Bull. Electr. Eng. Informatics*, vol. 11, no. 5, pp. 2460–2470, 2022, doi: 10.11591/eei.v11i5.3949.
- [10] S. Khadija, E. M. Ouardia, and F. Abdelmajid, "Nonlinear backstepping control of a partially shaded photovoltaic storage system," *Indonesian Journal of Electrical Engineering and Computer Science*, vol. 29, no. 1, pp. 225–237, 2023, doi: 10.11591/ijeecs.v29.i1.pp225-237.
- [11] E. Radwan, K. Salih, E. Awada, and M. Nour, "Modified phase locked loop for grid connected single phase inverter," *Int. J. Electr. Comput. Eng.*, vol. 9, no. 5, pp. 3934–3943, 2019, doi: 10.11591/ijece.v9i5.pp3934-3943.
- [12] A. Glumineau, M. Hamy, C. Lanier, and C. H. Moog, "Robust control of a brushless servo motor via sliding mode techniques," *Bull. Electr. Eng. Informatics*, vol. 1, no. 4, pp. 295–304, 2007, doi: 10.1080/00207179308923039.
- [13] V. Bist and B. Singh, "A reduced sensor PFC BL-Zeta converter based VSI fed BLDC motor drive," *Electr. Power Syst. Res.*, vol. 98, pp. 11–18, 2013, doi: 10.1016/j.epsr.2013.01.006.
- [14] S. Sashidhar, V. G. P. Reddy, and B. G. Fernandes, "A Single-Stage Sensorless Control of a PV-Based Bore-Well Submersible BLDC Motor," *IEEE J. Emerg. Sel. Top. Power Electron.*, vol. 7, no. 2, pp. 1173–1180, 2019, doi: 10.1109/JESTPE.2018.2810506.
- [15] D. S. Nayak and R. Shivarudraswamy, "Solar fed bldc motor drive for mixer grinder using a buck-boost converter," *Bull. Electr. Eng. Informatics*, vol. 9, no. 1, pp. 48–56, 2020, doi: 10.11591/eei.v9i1.1667.
- [16] W. Li, G. Zhang, T. Pan, Z. Zhang, Y. Geng, and J. Wang, "A Lipschitz Optimization-Based MPPT Algorithm for Photovoltaic System under Partial Shading Condition," *IEEE Access*, vol. 7, pp. 126323–126333, 2019, doi: 10.1109/ACCESS.2019.2939095.
- [17] B. Singh, V. Bist, A. Chandra, and K. Al-Haddad, "Power quality improvement in PFC Bridgeless-Luo converter fed BLDC motor drive," *Conf. Rec. - IAS Annu. Meet. (IEEE Ind. Appl. Soc.)*, pp. 1–8, 2013, doi: 10.1109/IAS.2013.6682498.
- [18] R. Kumar and B. Singh, "Solar PV powered BLDC motor drive for water pumping using Cuk converter," *IET Electr. Power Appl.*, vol. 11, no. 2, pp. 222–232, 2017, doi: 10.1049/iet-epa.2016.0328.
- [19] S. Chandra, P. Gaur, and D. Pathak, "Radial basis function neural network based maximum power point tracking for photovoltaic brushless DC motor connected water pumping system," *Comput. Electr. Eng.*, vol. 86, pp. 1-21, 2020, doi: 10.1016/j.compeleceng.2020.106730.
- [20] E. E. A. Zahab, A. M. Zaki, and M. M. El-sotouhy, "Design and control of a standalone PV water pumping system," *J. Electr. Syst. Inf. Technol.*, vol. 4, no. 2, pp. 322–337, 2017, doi: 10.1016/j.jesit.2016.03.003.
- [21] J. Arfaoui, H. Rezki, M. Al-Dhaifallah, F. Elyes, and M. Abdelkader, "Numerical performance evaluation of solar photovoltaic water pumping system under partial shading condition using modern optimization," *Mathematics*, vol. 7, no. 11, pp. 1–19, 2019, doi: 10.3390/math7111123.
- [22] M. R. Bengourina, R. Mostefa, S. Saadi, and L. Hassaine, "PSO based Direct Power Control for a Multifunctional Grid Connected

Photovoltaic System," *Int. J. Power Electron. Drive Syst.*, vol. 9, no. 2, pp. 610–621, 2018, doi: 10.11591/ijpeds.v9.i2.pp610-621.

[23] K. K. Jha and M. N. Anwar, "Solar Photovoltaic based Brushless DC Motor Driven Water Pumping System using PSO-MPPT Algorithm," *2019 54th Int. Univ. Power Eng. Conf. UPEC 2019 - Proc.*, pp. 1–6, 2019, doi: 10.1109/UPEC.2019.8893591.

[24] H. Rezk, A. Fathy, and A. Y. Abdelaziz, "A comparison of different global MPPT techniques based on meta-heuristic algorithms for photovoltaic system subjected to partial shading conditions," *Renew. Sustain. Energy Rev.*, vol. 74, no. Aug, pp. 377–386, 2017, doi: 10.1016/j.rser.2017.02.051.

[25] K. P. Panda, A. Anand, P. R. Bana, and G. Panda, "Novel PWM Control with Modified PSO-MPPT Algorithm for Reduced Switch MLI Based Standalone PV System," *Int. J. Emerg. Electr. Power Syst.*, vol. 19, no. 5, pp. 1–17, 2018, doi: 10.1515/ijeps-2018-0023.

[26] F. K. Abo-Elyousr, A. M. Abdelshafy, and A. Y. Abdelaziz, "MPPT-based particle swarm and cuckoo search algorithms for PV systems," *Green Energy Technol.*, pp. 379–400, 2020, doi: 10.1007/978-3-030-05578-3\_14.

[27] C. C. Ahmed, M. Cherkaoui, and M. Mokhlis, "PSO-SMC controller based GMPPT technique for photovoltaic panel under partial shading effect," *Int. J. Intell. Eng. Syst.*, vol. 13, no. 2, pp. 307–316, 2020, doi: 10.22266/ijies2020.0430.30.

[28] C. S. Kumar and R. S. Rao, "Enhanced grey wolf optimizer based MPPT algorithm of PV system under partial shaded condition," *Int. J. Renew. Energy Dev.*, vol. 6, no. 3, pp. 203–212, 2017, doi: 10.14710/ijred.6.3.203-212.

[29] F. D. Murdianto, M. Z. Efendi, R. E. Setiawan, and A. S. L. Hermawan, "Comparison method of MPSO, FPA, and GWO algorithm in MPPT SEPIC converter under dynamic partial shading condition," *Proceeding - ICAMIMIA 2017 Int. Conf. Adv. Mechatronics, Intell. Manuf. Ind. Autom.*, pp. 315–320, 2018, doi: 10.1109/ICAMIMIA.2017.8387609.

[30] S. Mohanty, B. Subudhi, and P. K. Ray, "A new MPPT design using grey Wolf optimization technique for photovoltaic system under partial shading conditions," *IEEE Trans. Sustain. Energy*, vol. 7, no. 1, pp. 181–188, 2016, doi: 10.1109/TSTE.2015.2482120.

[31] F. -E. Lamzouri, E. -M. Boufounas and A. El Amrani, "A Robust Backstepping Sliding Mode Control for MPPT based Photovoltaic System with a DC-DC Boost Converter," *2018 International Conference on Control, Automation and Diagnosis (ICCAD)*, Marrakech, Morocco, 2018, pp. 1-6, doi: 10.1109/CADIAG.2018.8751449.

[32] Z. M. Ali, N. Vu Quynh, S. Dadfar, and H. Nakamura, "Variable step size perturb and observe MPPT controller by applying  $\theta$ -modified krill herd algorithm-sliding mode controller under partially shaded conditions," *J. Clean. Prod.*, vol. 271, pp. 1–29, 2020, doi: 10.1016/j.jclepro.2020.122243.

[33] A. Borni, A. Bouchakour, L. Zaghiba, A. Thameur, A. Lakhdari, and N. Bessous, "Optimization of the fuzzy MPPT controller by PSO for the single-phase grid-connected photovoltaic system controlled by sliding mode," *Proc. 2018 6th Int. Renew. Sustain. Energy Conf. IRSEC 2018*, 2018, pp. 1-7, doi: 10.1109/IRSEC.2018.8702873.

## BIOGRAPHIES OF AUTHORS



**Sabri Khadija** was born in 1990. She obtained the master's degree in Automatic, Signal Processing, Industrial Computing from Hassan first University, Settat, Morocco, in 2014. She is currently a Ph.D. student at the Research Laboratory in Engineering, Industrial Management and Innovation, Faculty of Science and Technology, Hassan first University. His research interests include monitoring the maximum power of photovoltaic (PV) systems in general, storage systems and pumped-storage systems, partially shaded and the injection of energy into the grid. She can be contacted at email: k.sabri@uhp.ac.ma.



**El Maguiri Ouadja** was born in Zagora, Morocco in 1975. He obtained a Master's degree in Electrical Engineering from Hassan II University in 2003. He obtained the Ph.D. degree from Mohamadia School of Engineering in Rabat 2010 in Science and Technology. He is currently Professor of Electrical Engineering at CPA, CRMEF Casablanca-Settat, Morocco. He is member of the Laboratory of Engineering, Industrial Management and Innovation (IMII). He can be contacted at email: elmaguiriouadja@gmail.com.



**Farchi Abdelmajid** Ing Ph.D. in Electronic and Telecommunications Chiefs of research team Signals and Systems in Laboratory of Engineering, Industrial Management and Innovation. Educational person responsible of the Cycle Engineer Telecommunications and Embedded Systems to the Faculty of the Sciences and Technology of Settat, Morocco. He can be contacted at email: abdelmajidfarchi1@gmail.com.